Theor Chem Acc (2006) 116: 87–105
DOI 10.1007/s00214-005-0030-z

REGULAR ARTICLE

Marco Garavelli

Computational organic photochemistry: strategy, achievements and perspectives

Received: 31 March 2005 / Accepted: 28 September 2005 / Published online: 6 January 2006

Abstract In recent years, computational photochemistry has achieved increasing consideration as a valid tool for the investigation of photochemical reaction mechanisms in organic chromophores. A theoretical chemist can now adapt his/her "instruments" to the subject under investigation, as every other scientist does when there is a problem to study and a methodology to be chosen. Thus, different computational strategies and tools can now be operated like a *virtual spectrometer* to characterize the photoinduced molecular deformation and reactivity of a given chromophore, so that a full description of the reactive process (i.e. its reaction coordinate) *from energy absorption to photoproducts formation* can be achieved. Here we will review the basic concepts, the computational strategy and the theoretical tools, which permit this thorough description to be realized. Applications to the biologically and technologically relevant problem of photoinduced isomerizations in non-polar and highly polar conjugated polyenes will be shown, including also environment effects. Recent advances in this area (namely external charge effects) will be presented, together with new computational approaches, which allow molecular systems of biological size (*e.g.* the rhodopsin photoreceptors) to be investigated at an unprecedented level of accuracy. This should open the way to the accurate investigation of sizable systems in realistic conditions, providing chemists with information that might be used in molecular technology as a guideline for the design of artificial photoswitchable devices and the control of their photoinduced processes.

Keywords Conical intersection · CASSCF · CASPT2 · Ab initio · Photoisomerization

1 Introduction

The design and use of *molecular devices* behaving the way we want them to react to a certain external signal (by displacing, usually reversibly, one or more of their parts) represents a challenging and promising task in molecular technology (or else termed *nanotechnology*) [1]. Among the many molecular devices, those systems characterized by reversible reactions that can be photo-controlled are of a great interest. These devices are operated by irradiating the molecule at the proper wavelength required to trigger the photochemical process. In general, the design of the right reagent allows for a direct control of the reaction rate, efficiency and photostability even when the interconversion between the two (or more) "states" of the device needs to be repeated over a large number of cycles [2–5]. It is apparent that the elucidation of the factors regulating and controlling these reactions is imperative for the rational design of photo-switchable molecular systems that fit our needs (e.g. absorbing light of the proper wavelength or reacting with the desired rate and quantum yields) and for devising new photo-induced processes.

To achieve this goal, it is mandatory to know each detail of the reaction mechanism: this motivates *computational photochemistry*. In this review, we shall outline some of the recent achievements in this area (partly due to our group), focusing on minimum energy paths (MEP) [6] and the electronic structures encountered along the way. The aim is to show how a reliable computational investigation of the photochemistry of an organic chromophore can be achieved nowadays through high-level ab initio quantum chemical computations and ad hoc optimization tools. The purpose of this review, eventually, is also to show the possibility for a theoretical chemist to adapt his/her "instruments" (i.e. the method, the approach, the level of accuracy) to the subject under investigation, as every other scientist does when there is a problem to study and a methodology to be chosen. Thus, different computational strategies and tools can now be operated like a *virtual spectrometer* to characterize the photoinduced molecular deformation and reactivity of a given chromophore.

The computational approach used to accomplish this study is to follow the course of the reaction induced by light, by locating and characterizing the photochemical pathways (in terms of MEP) pursued by the molecular system along the potential energy surfaces (PES) of the photochemically relevant

M. Garavelli
Dipartimento di Chimica, "G. Ciamician" dell'Università di Bologna, Via Selmi 2, 40126 Bologna, Italy
E-mail: marco.garavelli@unibo.it

states, from the Franck Condon (FC) point on the spectroscopic state to the decay to the ground state and to the photoproducts. Such an approach has been named the *photochemical reaction path* or, more briefly, *pathway* approach [7,8]. Within this approach one pays attention to local properties of the potential energy surfaces such as slopes, minima, saddle points, barriers and crossings between states (see Sect. 2). The information accessible with this method is structural, the calculated MEP referring strictly to the path traveled by a vibrationally cold molecule that moves with infinitesimal kinetic energy. This path obviously does not represent any "real" trajectory followed by any "hot" molecule (for recent reviews and papers on non-adiabatic reaction dynamics the reader is encouraged to see [9–29]; a diabatic representation [30–36] is often found more convenient in this case) still it supplies essential information about the slopes, basins, barriers and valleys experienced by the system during its motion. Moreover, it allows the rationalization of a series of experimental data, e.g. excite-state lifetimes, nature of the photoproducts, quantum yields, transient absorptions and emission bands (spectra). This approach can be closely related to the common way of describing photochemical processes with the motion of the center of a wave packet along the potential energy surfaces [37].

The energy surface structural features and, ultimately, the entire reaction path are computed by determining the molecular wave function with state-of-the-art ab initio methods. While in the past few decades ab initio quantum chemical and (following their impressive development) density functional methods have been widely and successfully applied to the investigation of the reactivity of molecules in their electronic ground state [38,39], the corresponding development for excited states has been slower. One reason is the larger complexity of an excited state wave function: the electronic ground state for most systems close to their equilibrium geometry is well described by a single electronic configuration, but this is not the case for the excited states. Here, different electronic configurations have to be accounted for since they are often close in energy and mix heavily, i.e. the wave function is a linear combination of such configurations. It is often difficult to decide a priori which configurations will be important in a given situation. The multi-configurational approach [40] avoids this decision by dividing the orbitals into three sets: inactive, active, and secondary orbitals. While the inactive (secondary) orbitals are doubly occupied (are empty) for all the considered electronic configurations, the remaining (n_a) orbitals are active and are chosen according to the specific chemical problem we are interested in. There are typically less than $2n_a$ electrons housed in the active orbitals, therefore they can give rise to a number of excited configurations. A linear combination of these originates the excited state wave function of interest. Indeed the method is called *complete active space self consistent field* (CASSCF) [40–42] since it computes all the configurations within the given active space, optimizing the linear combination coefficients, together with the orbitals included in the active and inactive space [40–42]. Although far from being a black-box tool (i.e. skills, decision making and supervision is needed), the extensive testing carried out over the years has shown that the CASSCF method yields an efficient mapping of the topography of the reactive excited state potential energy surfaces, permitting the analytical evaluation of gradients and second derivatives. Furthermore it is available in widely distributed software packages such as *Gaussian* [43] and *MOLCAS* [44]. On the other hand, energies may still not be accurate enough since it does not fully account for the *electron correlation energy*. Therefore, in order to refine the energetics by including electronic correlation, a multireference-MP2 method (such as, for example, the CASPT2 [45,46] or multi-state CASPT2 [47] included in *MOLCAS* (that takes the CASSCF wave function as the zeroth-order wave function), or the quasidegenerate approach of Nakano and Hirao [48] which may be more appropriate, as for the similar multi-state CASPT2 approach, near an intersection or avoided crossing) can be employed. A combined CASPT2//CASSCF methodology has been extensively used by us since it was proven to reproduce data with experimental accuracy (i.e. errors within 3 kcal mol^{-1}) [8,49]. Below we will focus on the results of this approach (for the systems documented here, a 6–31G* basis set has always been used since it produces reliable results), although it is not the only one available for excited state reactivity studies. In principle, every method that allows for a correct evaluation of the excited states energy, gradient and Hessian with respect to the geometrical coordinate of the reactant may be used for this purpose.

Another serious point we need to face is that a photochemical process (where the reactant typically resides on an excited state PES and the products accumulate on the ground state) is expected to have two branches: one located on the excited state and the other located on the ground state potential energy surface. The main difficulty associated with such a computation lies in the correct definition and practical computation of the *funnel* where the excited state reactant or intermediate is delivered to the ground state. Thus, during the last decade, computational chemists have been able to develop novel tools and strategies to solve this fundamental problem [40,49–56]. In particular, a systematic computational investigation of a wide range of photochemical organic reactions has led to novel concepts (e.g. conical intersection (CI) funnels, photochemical and quenching paths, path branching and selectivity) that allow the definition of the photochemical reaction mechanism in a rigorous way and with a language familiar to chemists. The goal is the complete description of what happens at the molecular level *from energy absorption to product formation* (i.e. the full description of the reaction path) and here we will review the theoretical tools (partly developed by our group), which permit this thorough description to be achieved (see Sect. 3).

Applications to the photoinduced isomerizations in nonpolar and highly polar polyenes (e.g. the *cis–trans* photoisomerizations in conjugated olefines and protonated Schiff bases – PSB – of polyenals, and the photoinduced processes involving conjugated cyclic hydrocarbons which are relevant,

for instance, to photochromism) will be discussed in Sects. 4–7. These chromophores have extended conjugated π-systems and may be characterized by ultrafast and efficient isomerizations taking place upon photoexcitation. These systems are relevant in photobiology (e.g. carotene and previtamin-D photochemistry, while the PSB of retinal is the chromophore of an important family of photoreceptors, i.e. the rhodopsin proteins) and can be potentially employed in nanotechnology for the design and construction of molecular devices such as random access memories, photon counters, picosecond photo detectors, neural-type logic gates, optical computing, light-switchable receptors and sensors, light addressable memories, molecular switchers and molecular motors just to mention a few [2,57,58]. In addition, recent advances in the understanding of environment effects will be reviewed in Sect. 6 where external charges will be shown to affect and tune PSB photochemical reactivity. Finally, our recent steps toward a computational photobiology will be documented by presenting a recently developed QM(CASPT2//CASSCF)/MM(Amber) hybrid force field (Sect. 3) that allows molecular systems of biological size (e.g. photoreceptors) to be investigated at an unprecedented level of accuracy. Recent applications to rhodopsin proteins will be presented (Sect. 8), and the new frontiers, challenges and perspectives for an accurate ab initio computational investigation of photochemical processes in sizable systems of biological and supramolecular relevance will be discussed.

2 Conical intersections in photoinduced processes

The classic text-book view of photochemical reactions is mainly due to the 1969 computational work of Van der Lugt and Oosteroff [59]. These authors proposed the decay of an excited species taking place at an excited state energy minimum corresponding to an *avoided crossing* of the excited and ground state potential energy surfaces (Scheme 1a). In polyatomic molecules, the crossing of PES is not avoided everywhere. The intersection space of two n-dimensional PES of the same multiplicity is $(n-2)$-dimensional and the crossings have the shape of a double cone (hereafter named as conical intersection) if plotted versus the two remaining coordinates of the "branching space" (see e.g. [54]). Zimmerman [60], Teller [61] and Michl [62] were the first to suggest, independently, that certain photoproducts may originate by decay of the excited state species through a CI of the excited and ground state potential energy surfaces (Scheme 1b).

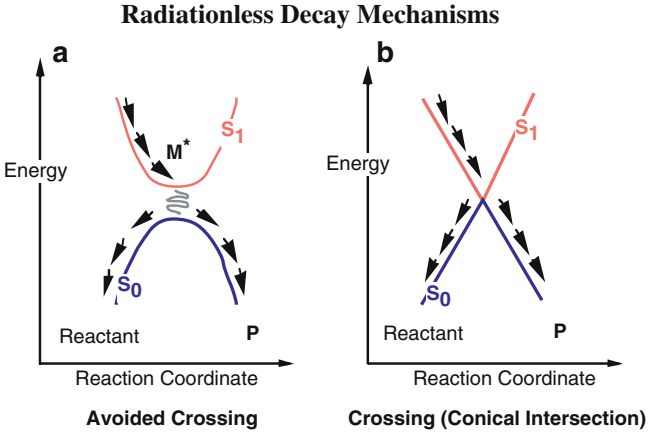

Scheme 1 Radiationless decay mechanisms (from [63])

Although this has long been known and the commonality of CIs has already been appreciated (on the basis of purely theoretical considerations) by a restricted audience of theoretical chemists (see [64] for a review), it was only recently found after the development of efficient localization algorithms [65], that such CIs are ubiquitous in photochemistry (see e.g. [49,54]). Nearly two decades of systematic computational studies have shown that low-lying CIs represent a general mechanistic entity in photochemistry, playing a central role in this field in analogy with transition states for thermal reactions [8,49,56]. Consequently, an excited state has a high probability of entering a region where the excited state crosses the ground state. Such crossings provide a very efficient *funnel* for radiationless deactivation (i.e. internal conversion), which may occur in a single molecular vibration (i.e. in a subpicosecond timescale) and, in turn, prompt photoproducts formation. In fact, the upper cone acts as a collection funnel, whereas on the lower cone the reaction path can branch toward the product(s) and reactant, so that the quantum yield will largely be formed there. These results imply that when two or more surfaces are considered in the exploration of a photo-process, some reaction path features are expected. In summary one expects:

- the existence of an accessible funnel corresponding to a CI connecting the excited to the ground state branches of the reaction path;
- the overall excited state motion is guided by the MEP (i.e. a steepest descent path) and therefore by local structural features of the potential energy surfaces;
- the branching of the reaction path at the position corresponding to the CI, leading to the final photoproducts or back to the original reactant via two or more ground state relaxation paths.

Radiationless decay at a CI implies: (a) a 100% efficient internal conversion (i.e. the Landau–Zener [52,54] decay probability will be unity) that makes the intersection a structural bottleneck for the reaction (as recently shown by Jasper and Truhlar [11] and Jasper et al. [14] this may be seen as an oversimplification since real trajectories explore wide regions around the crossing seam but essentially never go through this seam and one often needs to consider a much wider region of the surface than just a point of crossing: the reader is alerted to this cautionary view), (b) a slow decay rate (e.g. the competition with fluorescence) may reflect the presence of some excited state energy barrier which separates the excited state intermediate M* from the intersection structure CI (Fig. 1) and (c) in the case where the decay leads to a chemical reaction, the molecular structure at the intersection must be related to the structure of the observed photoproducts (P), as in thermal reactions the structure of the transition state is related to that of the products.

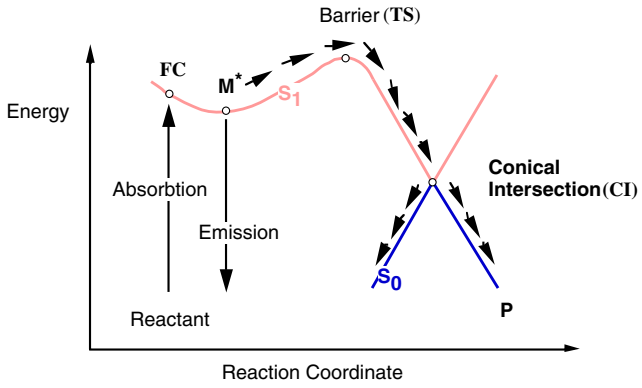

Fig. 1 Schematic reaction path for a barrier controlled "opening" of a fast radiationless decay channel (from [63])

Points (a)–(c) presented above provide the theoretical basis for the modeling of photochemical reactions or, in other words, for computational photochemistry. The molecular motion is assumed to be controlled by the structure of the relevant excited and ground state potential energy surfaces. Thus, information on the excited state lifetime and on the type of photoproducts generated is obtained by computing and analyzing the reaction coordinates and energies (i.e. the reaction path) connecting *the Franck-Condon point, to the excited state intermediate* M* *(if existing) and to the ground state*. In conclusion, the strategy used is based on the mapping of the photochemical reaction path computed by following the MEP from the starting (e.g. Franck-Condon structure FC) to the final (e.g. ground state photoproducts P′ and P″) points *through*, for example, a CI.

We must emphasize that the MEP procedure has the big advantage not to constrain the molecule to any specific spatial symmetry or internal coordinate (i.e. fully unconstrained optimizations are performed): the system is fully free to relax on the PES of the photochemically relevant states, *naturally* finding its way out to the deactivation funnel (i.e. the CI) and the final photoproducts. This provides a more accurate insight into the photochemical process than other more standard and classical techniques do such as, for example, *surface-scanning* and *surface-cross section* methods. One limit of these two approaches is that the PES is mapped along a pre-defined reaction coordinate. Thus, so doing, the CI funnel can be missed and an avoided crossing misleadingly found in its place: this was the case for the Van der Lugt and Oosteroff [59] radiationless decay model (see Scheme 2).

3 Computational tools

Standard methods for molecular structure optimization of stationary points as well as for computing MEP (e.g. the intrinsic reaction coordinate (IRC) method) [66] are employed for the mapping of both the ground and the excited states. However, description of the crossing region requires special methods as two potential energy surfaces become degenerate and the gradient and Hessian cannot be unambiguously computed. These

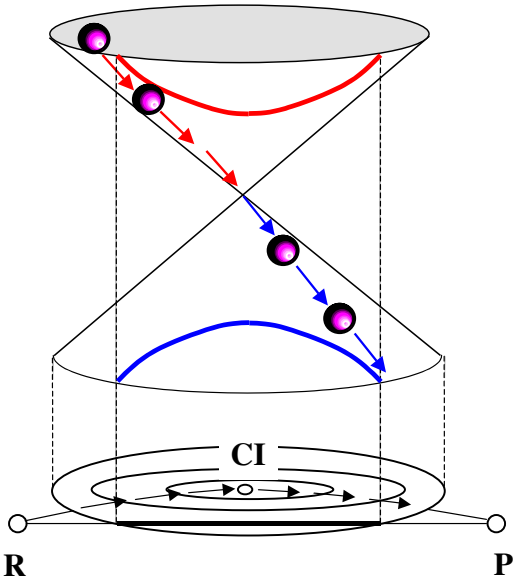

Scheme 2 (From [8])

tools are currently available in standard software packages such as Gaussian *03* [43] and will not be presented here since they have recently been discussed in previous reviews [67, 68]. In contrast, below we will focus on the *branching* of the photochemical reaction path occurring upon decay from a higher to a lower laying state. The inter-state nature of such paths requires special methodologies to locate the energy valleys describing the relaxation process (e.g. the ground state relaxation following decay at the crossing). Methods for computing relaxation paths starting from a crossing point (or, more generally, from non-stationary points) are still matter of research and to our knowledge are not yet distributed.

3.1 Locating relaxation paths from a conical intersection

As mentioned above, an accessible CI forms a structural bottleneck that separates the excited state branch of a photochemical reaction path from *one or more* ground state branches connecting the excited state reactant to one or more ground state products (Fig. 2). The number and nature of the products generated following decay at a surface crossing will depend on the population of such branches, each one corresponding to a different relaxation path. We have recently implemented a gradient-driven algorithm [69,70] to locate and characterize all the accessible branches via the calculation of the initial relaxation directions (IRD) departing from a single conical intersection point. The MEP starting along these relaxation directions correspond to the possible relaxation paths which, in turn, locate the ground state valleys developing from the intersection region and comprising the energy minima of the corresponding photoproducts. Thus, by connecting the excited state and ground state paths a full description of the photochemical process *from energy absorption to photoproduct formation* may be accomplished.

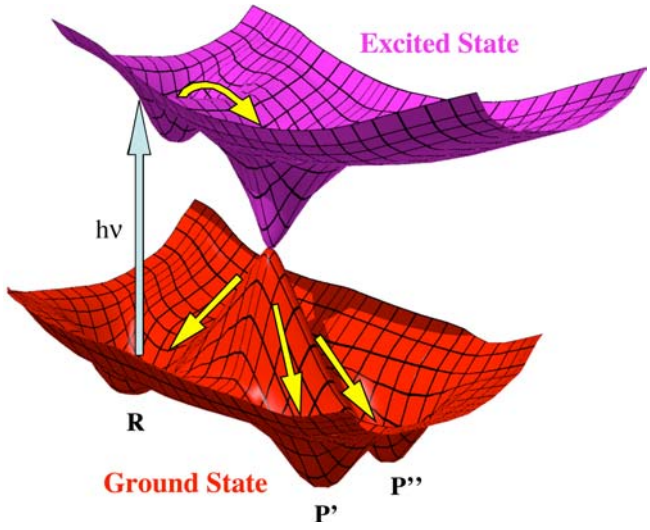

Fig. 2 Photochemical relaxation path branching, leading (via conical intersection (CI) decay) to three different final structures: two photoproducts $\mathbf{P}'$ and $\mathbf{P}''$ and the starting reactant **R**

The procedure adopted to carry out these IRD and MEP computations is reported in [65,70] and is summarized here. Briefly, an IRD corresponds to a local *steepest descent direction*, in *mass-weighted co-ordinates*, from a given starting point. The IRD is calculated by locating the energy minimum on a hyperspherical (i.e. $n-1$ dimensional) cross-section of the n dimensional PES (n is the number of vibrational degrees of freedom of the molecule) centered on the starting point (the CI in this case). The radius of this hypersphere is usually chosen to be small (typically 0.25–0.5 au in *mass-weighted co-ordinates*) in order to locate the steepest direction in the vicinity of the starting point (which corresponds to the hypersphere center). The IRD is then defined as the vector joining the starting point to the energy minimum (an *hyperminimum*). Once the *hyperminima* have been determined, the associated MEP (emerging from these points) is computed as *the steepest descent line in mass-weighted co-ordinates* (au $=$ amu$^{1/2}$a$_0$) using the IRD vector to define the initial direction to follow. The standard IRC method [66] can be used for that purpose. As a consequence, the approach outlined above provides a systematic way to find the MEP connecting the vertex of the cone to the various ground state photoproduct wells.

Although this methodology has been presented for the case of ground state reaction paths departing from a conical intersection, it may also be used to locate paths beginning from a different non-stationary point, such as the FC point, for example. In conclusion, a two-step strategy for the computation of the full photochemical reaction path is requested. Within the first step, keeping to the MEP from the FC region, key structures like minima and CI can be located. In the second step, the MEP describing the S_0 relaxation process from the CI (determined in the first step) are calculated with the strategy outlined above and the paths leading to the various photoproducts determined.

3.2 Moving towards photobiology: a hybrid quantum mechanics (QM)/molecular mechanics (MM) approach to photochemistry

The influence of the environment (e.g. solvent and the protein cavity) on the mechanism of these photoinduced reactions could be quite strong if not dramatic, but it is still largely misunderstood. In addition, understanding these effects is mandatory for applications in molecular technology where the chromophores do not behave as isolated entities in gas-phase, but are reacting in a suitable environment and are connected to other molecular systems surrounding (and affecting!) them. For example, protein-bound and free-solution retinal PSB show different photophysical and photochemical features. More specifically, the protein environment (e.g. rhodopsin (Rh) and bacteriorhodopsin (bR)) modifies the chromophore spectroscopic properties and, most important, accelerates the reaction ratio and controls its stereochemistry.

In order to rationalize these "catalytic" effects, a detailed mechanistic study of the photoinduced process in protein has to be done. Given the extension of the system, it is impossible to describe the whole protein and the chromophore at the high ab initio level required to catch the fine details of the reaction mechanism. A good compromise between accuracy and computational cost is to develop a hybrid quantum mechanics/molecular mechanics (QM/MM) method, which describes the reactive molecule (e.g. the retinal chromophore) at a suitable QM level, while the rest of the environment (e.g. the solvent and/or the protein cavity) is described via a classic MM force field (for general references on QM/MM methods in the treatment of adiabatic reactions see [71–73]). Thus, we describe *quantum mechanically* the *electronically important region* of the system (i.e. the part which undergoes the chemical reaction), while the environment effects are described using a less expensive *molecular mechanics* method. Several approaches have been developed, since many different QM and MM methods can be coupled in following various schemes, and the link between the QM and MM regions can be the subject of different types of approximations. As a basis for our QM/MM parameterization, we choose the Amber force field for the MM part and the CASSCF for the QM part. CASSCF has been chosen because one is interested in describing as accurately as possible the molecular evolution of the chromophore on the photochemically relevant excited states, and a CASPT2//CASSCF computational strategy has been shown to do that (as discussed in the sections above).

The QM/MM force field is characterized by a special Hamiltonian, which is the sum of three terms:

$$\hat{\mathbf{H}} = \hat{\mathbf{H}}_{\mathrm{QM}} + \hat{\mathbf{H}}_{\mathrm{MM}} + \hat{\mathbf{H}}_{\mathrm{QM/MM}}$$

On the right hand side, $\hat{\mathbf{H}}_{\mathrm{QM}}$ is the usual Hamiltonian of the QM part as if it were in vacuo, $\hat{\mathbf{H}}_{\mathrm{MM}}$ is actually the classical energy of the very MM part only and $\hat{\mathbf{H}}_{\mathrm{QM/MM}}$ takes into account all the interactions between the QM and MM subsystems. Given n electrons and N nuclei interacting with Q point charges, this last term can be split into several contributions:

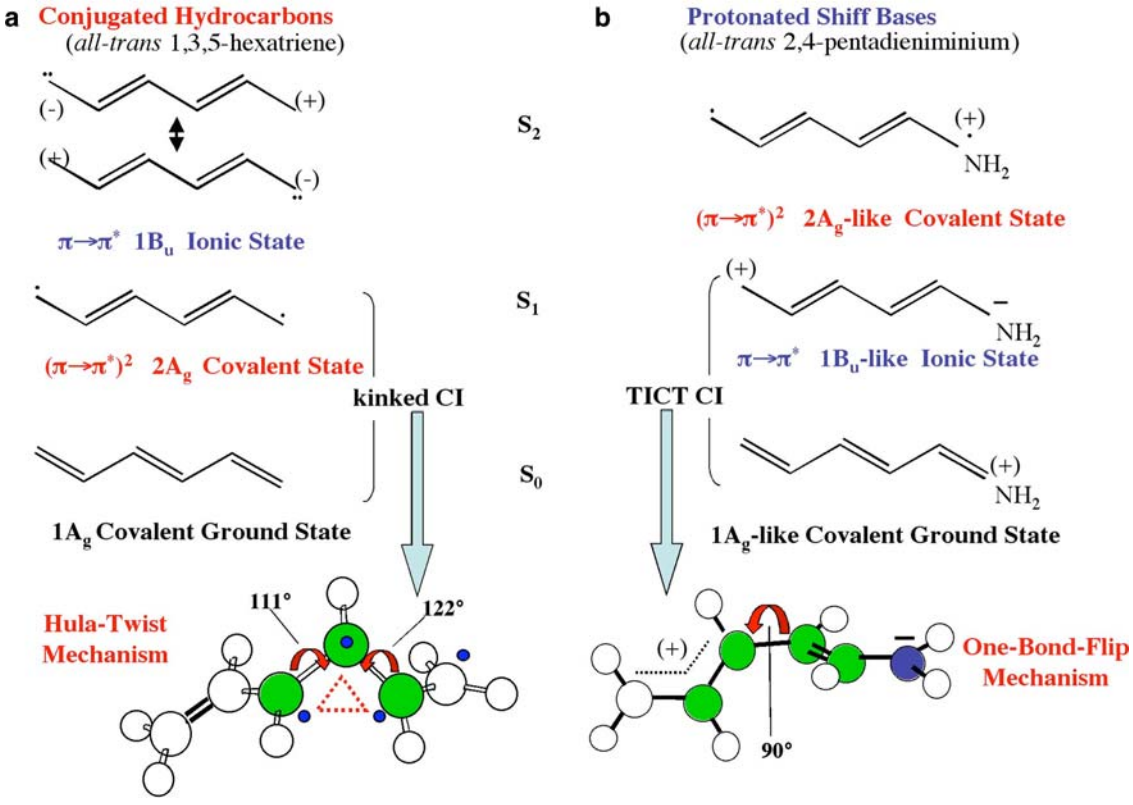

Scheme 3

$$\hat{\mathbf{H}}_{\mathrm{QM/MM}} = \sum_{i=1}^{n}\sum_{j=1}^{Q}\frac{-q_j}{r_{ij}} + \sum_{i=1}^{N}\sum_{j=1}^{Q}\frac{Z_i q_j}{r_{ij}} + E_{vdW} + E_{\mathrm{bonded}}$$

Briefly, the MM and QM segments interact in the following way: (a) the QM electrons and the full set of MM point charges (which are described by the original atom-centered restrained electrostatic potential (RESP) [74] point charges in the Amber force field) interact via the one-electron operator (i.e. the first term of the equation above, which ensures that the QM wave function is polarized by all the surrounding point charges), (b) the electrostatic interactions between the QM nuclei and the full set of MM point charges are computed by the second term of the QM/MM Hamiltonian, (c) QM and MM atom pairs separated by at least three bonds interact via either standard or reparameterized van der Waals potential and (d) stretchings, bendings and torsions at the QM/MM frontier are described by the standard MM potential (we choose to take into account all classical interactions involving at least one MM atom). Please note that while in Amber, electrostatic and van der Waals interactions are computed when two atoms are separated by at least three bonds, our QM subsystem feels all the MM point charges.

Since this method computes the electrostatic interactions between atoms by making use of the atom-centered RESP charges, we validated this QM/MM approach by reproducing the results obtained at a fully QM base for model systems. In particular, since we are interested in Rhodopsin photoreceptors, this validation has been performed on an ionic pair similar to that found for the retinal PSB chromophore and its counter ion in Rhodopsins. Furthermore, to achieve the best accuracy and minimize the atom-link approximation effects, the method is based on a carefully reparameterized hydrogen link-atom scheme, which is described in detail in [75]. This makes the designed QM/MM force field to be strongly problem dependent but highly accurate. Finally, the CAS calculations are based on an active space that comprises the full π-system of the chromophore.

4 Nonpolar versus polar conjugated systems

The singlet manifold for the relaxed structures of linear nonpolar conjugated olefins (Scheme 3a) and the isoelectronic highly polar PSB of the corresponding polyenal (Scheme 1b) is shown in Scheme 3 (the all-trans hexatriene and pentadieniminium cation are used as an example). As we already know both from the experiments [76] and the computations [8,54,69,77–83], the lowest relaxed singlet excited state (S_1) in conjugated nonpolar olefins is the dark (i.e. the $S_0 \rightarrow S_1$ transition is symmetry-forbidden) two-electron excited (π*2) 2Ag state which is covalent (it has a diradical – dot–dot – nature) as is also the ground state (1Ag), while the bright (i.e. spectroscopic) one-electron excited ($\pi\pi$*) 1Bu state is ionic (it is dominated by two dipolar – hole-pair – mesomeric structures) and is higher (S_2) in energy. Therefore, low-lying two-electron excited (2Ag) states play a central role in the singlet photochemistry of nonpolar polyenes because molecules tend

to pass through them before reaching the ground state surface [54]. That is, these S_1 surfaces collect the population from the initially excited (S_2) states ($S_2 \rightarrow S_1$ relaxation is very efficient and occurs in an ultrashort time (50–200 fs)) [84], driving the photochemistry of the system and controlling the outlets of the process.

The NH_2^+ group is a stronger electron-withdrawing group than CH_2. Hence, introduction of this charged group at one end of a polyene, such as in retinal PSB or similar molecules, will stabilize the charge transfer $\pi\pi^*$ state (while destabilizing the π^*2 state), since nitrogen can accommodate much better than carbon the electronic lone pair. If this effect is big enough, the order of the two relaxed low energy singlet excited states will swap. Calculations show that this is in fact the case for PSB in isolated conditions: in such molecules [85–87], in contrast to polyenes [54], the ionic charge-transfer 1Bu-like singly excited ($\pi\pi^*$) state gets below the diradical-type 2Ag-like two-electron excited (π^*2) state. One can therefore expect a difference in the photochemistry of highly polar double-bond systems compared to nonpolar ones, since the relaxed photochemically relevant excited states S_1 has changed in nature. For example, since S_0 and S_1 in neutral polyenes are both covalent states that belong to the same symmetry (Ag), mixing and interaction between these states is allowed in general, and all bonds have a certain π-bonding character also in the relaxed 2Ag state (i.e. the 'diradical-type' S_1 minimum), due to a partial contribution of the valence-bond closed shell configuration [88]. That is, conjugated polyenes have a well defined *planar minimum* in their first excited state, as has been established spectroscopically [76] and computationally [54,77–79]. On the other hand, S_1 in PSB corresponds to a charge-transfer one-electron excited state that is 1Bu-like (i.e. it would have this symmetry if N^+ and C would not be distinguished). This excited state, which is the lowest one as mentioned, will therefore interact only very little with the ground (2Ag-like) state and will hence have its relaxed planar structure (not necessarily a minimum any more) at the geometry expected for just this mesomeric structure. Hence from this state, one-bond flip (OBF) around a former double bond (that now has become a single-bond) will be much easier than in a nonpolar polyene (where, according to the computations, significant energy barriers are involved [79,89]). This difference is in fact confirmed by our detailed computational investigations [85–87], that show substantially barrierless paths for the OBF photoisomerization of the internal double bonds in isolated PSB.

Another interesting difference concerns the form of the low lying conical intersections, which provide the outlets of the excited state paths, and largely control the QYs (branching ratios) and the product manifold of the photochemical process. As mentioned above, the OBF photoisomerization process involving the internal double bonds is barrierless in isolated PSB. These bonds become C–C single bonds in this state (as seen above), but are C=C double bonds in the ground state. Therefore, while S_1 is stabilized upon rotation, the ground state S_0 is destabilized concurrently and the two surfaces may intersect. These crossings have indeed been found [85–87] and have the form of a twisted intramolecular charge transfer (TICT) state (see Scheme 3b). Such CI can already be predicted by the "two-electron two-orbital model" of Michl and Bonacic-Koutecky: according to this theory, the geometry of the two nearly perpendicularly twisted allyl-like fragments can be adjusted to make the ionization potential of the CH2CHCH- SOMO and the electron affinity of the $-CHCHNH2^+$ SOMO to become equal. This makes the charge transfer (hole-pair) S_1 and the covalent (diradical dot–dot) S_0 states to become degenerate since their energy separation is given by the difference between these two quantities. This interpretation has been strongly supported by our computations. In neutral polyenes, on the other hand, the intersecting S_1 and S_0 states are both covalent and the resulting CI have a typical polyradicaloid (i.e. tetraradical) character which gives rise to completely different geometrical features as, for example, the kink [77,90], i.e. an out of plane triangular structure that has been found in linear and cyclic neutral polyenes and has been interpreted as a three-electron/three-center bond (see Scheme 3a) that can gives rise to degeneracy of the two electronic states. The recoupling patterns between the uncoupled electrons of these polyradicaloid CI will characterize ground state relaxation channels and drive photoproducts formation.

5 Prototype conical intersections in nonpolar conjugated hydrocarbons

In our past works we have provided evidence that low energy covalent(S_1)/covalent(S_0) conical intersections in nonpolar polyenes may exist according to three different geometric and electronic arrangements, corresponding to different tetraradical-type interaction patterns such as thetrahedral (Scheme 4a), rhomboid (Scheme 4b) and triangular (Scheme 4c). In the past [91] the same patterns and conical intersections have been documented in an elementary system such as the H_4 clusters. The low-energy conical intersection driving cyclooctatetraene photochemistry represents an example of a tetrahedral interaction scheme (see Scheme 4a) [92,93]. The four unpaired electrons of the low-energy conical intersections found in 2,3-di-*tert*-butyl-buta-1,3-diene [81] and in the ethylene–ethylene cycloaddition [70] interact according to a rhomboid pattern (see Scheme 4b), while benzene, cyclohexadiene and linear conjugated chains in general have triangular-type low-energy conical intersections (see Scheme 4c) [69,77,79,89,94]. As clearly shown in Scheme 4, each prototype conical intersection has its specific recoupling scheme on the ground state. Thus, a rhomboid pattern may prompt the simultaneous formation of two new σ-bonds (leading to bicyclobutane via a one-step concerted mechanism) [81]. On the other hand, $-(CH)_3-$ kinked intersections may prompt both *cis*→ *trans* photoisomerizations and 1–3 σ-bond formation (leading, for example, to cyclopropanation reactions), as seen in benzene, cyclohexadiene, linear polyenes [69,77,79,89,94]. Finally, tetrahedral interaction may promote transanular bond formation such as the C_1–C_5

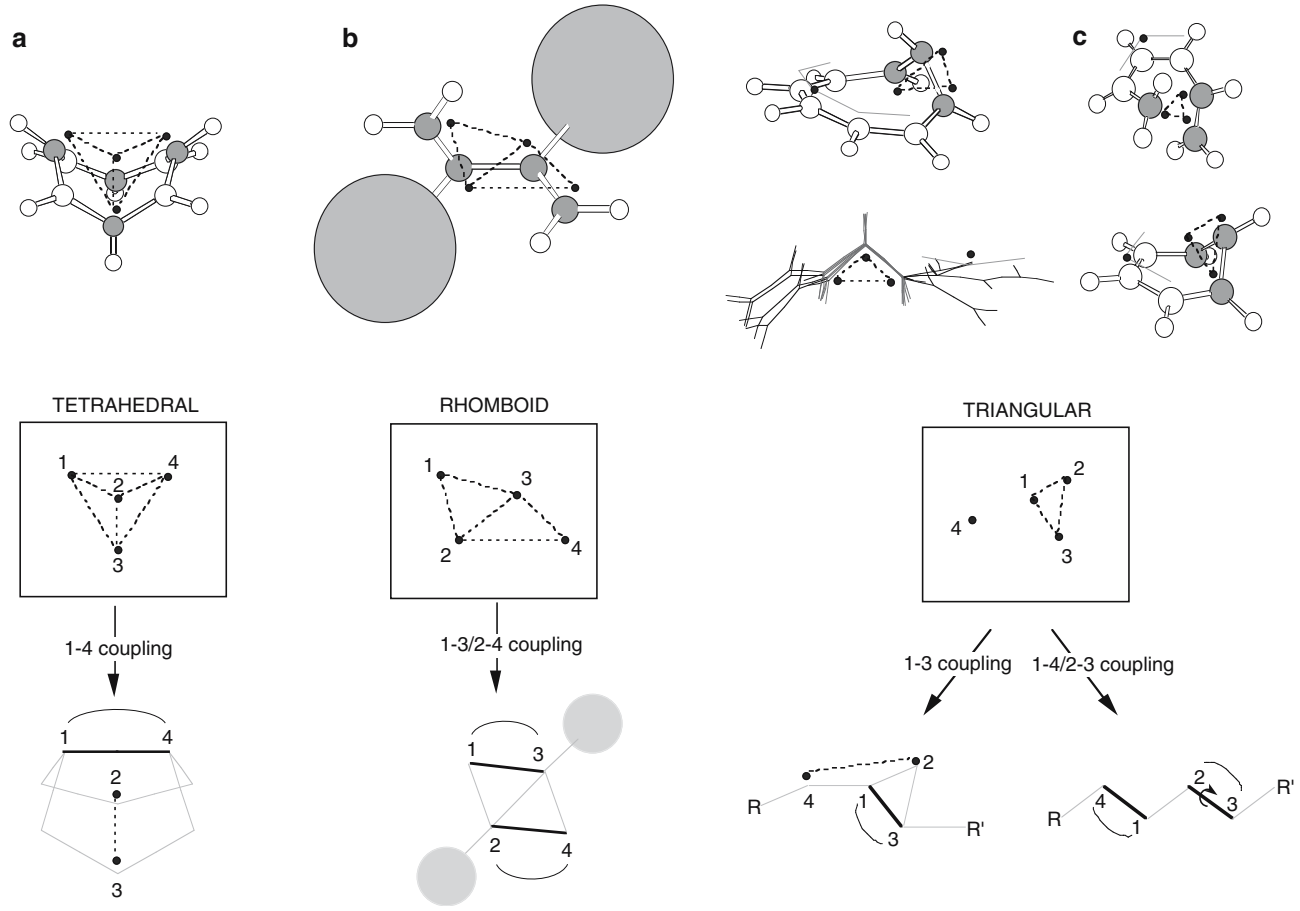

Scheme 4 (From [93])

photoinduced bond formation in cyclo-octatetraene, leading to semibulvalene.

A major task in our study is to understand and rationalize the factors playing a role in the selection and stability of low-energy conical intersections. As discussed above, each structure controls the outcome of a photochemical process. Thus, the knowledge of a simple predictive model could provide a valuable guideline for designing selective photochemical processes leading to complex molecular architectures (e.g. polycyclic carbon backbones) through irradiation of simple conjugated hydrocarbons [95]. Examples of these processes are the production of bicyclobutanes from butadienes [96], tetrahedranes from cyclobutadienes [97], benzvalenes from benzenes [98] and semibullvalenes from cyclo-octatetraenes [99–101]. A simple question may help us to catch the issue: why do cyclic systems such as benzene (an aromatic hydrocarbon) and cyclohexadiene (and in general linear conjugated hydrocarbons) decay through a low-energy $-(CH)_3-$ kink conical intersection, while in cyclooctatetraene the favored reactive funnel corresponds to a different prototype (i.e. tetrahedral, see Scheme 4) crossing?

An answer may be found for conjugated cyclic systems via a systematic analysis of all the possible *low-energy* covalent valence-bond (VB) configurations, which come by arranging the four unpaired electrons of a conical intersection in the π-system [93]. While for benzene (as well as cyclohexadiene) the lower-energy arrangement may only involve *one* delocalized allyl radical and *three* adjacent unpaired electrons (i.e. the triangular kink, see Scheme 4c and 5a), in cyclo-octatetraene, due to its larger size, a new and more stable tetraradical-type configuration is possible. This configuration corresponds to the electronic structure found in $\mathbf{CI_b}$, and accommodates a tetrahedral interaction pattern (see Scheme 4a). Here, we have only *two* unpaired single-centered (C_1, C_5) electrons, plus *two* delocalized allyl radicals (see Scheme 5b). Obviously, this configuration is electronically more favored than the kinked (triangular) one ($\mathbf{CI_b}$), where three unpaired electrons are localized on adjacent carbon centers (C_1, C_2, C_3) and only one delocalized radical exists. Thus, in conclusion, it appears that the existence of different covalent configurations depends on the extension and flexibility of the system and, in turn, on the energy of the orbitals which accommodate the electrons.

By further extending the length of the ring (e.g. to cyclodecapentaene), we could end up with an even more stable tetraradical-type configuration for a conical intersection. This involves, according to our model, a four-centered interaction pattern with *three* singly occupied allyl orbitals and only *one* singly occupied carbon-centered π-orbital (see Scheme 5c). A second, less stable configuration involves only *two*

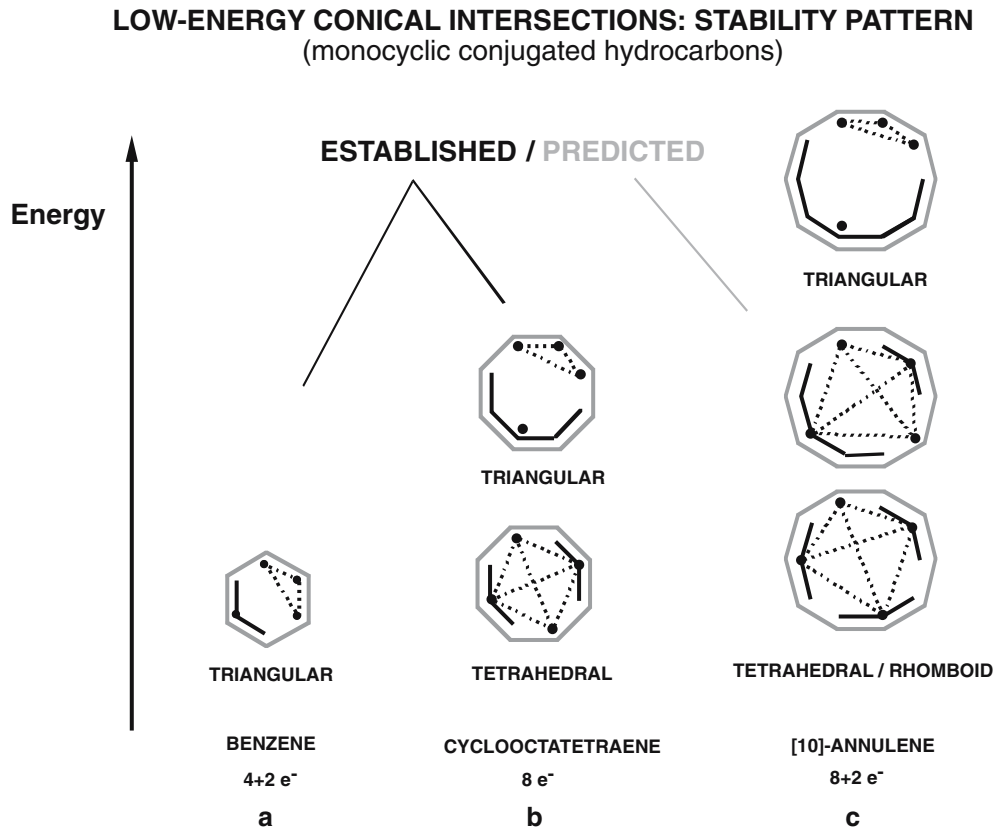

Scheme 5 Low-energy conical intersections: stability pattern (monocyclic conjugated hydrocarbons, from [93])

delocalized (an allyl and a pentadienyl) radicals and may generate a higher energy conical intersection structure. Finally, a third unstable configuration (with only *one* delocalized heptatrienyl radical) matches a triangular pattern, and therefore corresponds to the most unstable $-(CH)_3-$ kink crossing point. Provided these electronic effects are the only interactions involved (e.g. steric interactions are ca. equivalent for the different conical intersections), we should end up with the energetic order shown in Scheme 5c. On the other hand, unsubstituted linear conjugated systems (e.g. *all-trans* polyenes) can reach (from their side of the potential) only triangular type conical intersections (i.e. the $-(CH)_3-$ kinked crossing). For the other interaction patterns to occur, major conformational changes and flexibility are necessary.

Although qualitative, this picture seems to fit experimental and computational evidence, and could be of predictive value in the photochemistry of conjugated hydrocarbons. Moreover, this model may help us both to design and control ad- hoc photoinduced processes: via tuning the conditions which affect the stability of VB configurations (and therefore the related conical intersection structures) it could be possible, in principle, to select among different photoproducts patterns.

Accurate investigation of larger terms (such as cyclodecapentaene and longer polyene chains), complemented by exploration and characterization of the S_1/S_0 intersection space (i.e. the $n-2$ dimensional degenerate space), may shed new light on this fascinating area.

6 Conical intersections in psb

6.1 Isolated chromophores

The biological activity of rhodopsin proteins [102–107] is triggered by the ultrafast (200 fs in Rh) light-induced *cis–trans* isomerization of the retinal PSB chromophore, which induces a conformational change in the photoreceptor [102, 106]. Recently, we have reported the results of a series of ab initio multiconfigurational second-order perturbation theory computations for PSB models of different chain length in isolated conditions (i.e. in vacuo). These include, among the others, the minimal PSB model 2-*cis*-penta-2,4-dieniminium cation **1** [85], the all-*trans*-epta-2,4,6-trieniminium cation **2** [80], and the 11-*cis* (PSB11) and all-*trans* (PSBT) retinal chromophore models 4-*cis*-γ-methylnona-2,4,6,8-tetraeniminium **3** and all-*trans*-nona-2,4,6,8-tetraeniminium **4** cations, respectively [86,87,108]. As reported in [87], photoisomerization path computations on models **1**, **2**, **3** and **4** have provided a unified and unambiguous (although qualitative) view of the *intrinsic* (i.e. absence of environmental effects) photochemical reactivity of PSBs. Despite the different length of the conjugated chain (which quantitatively affects the spectroscopy and the energetic of the system) and the lack of the retinal β-ionone ring (which could play a role in the steric factors involved in constrained environments), it has been demonstrated that, in all cases, the photochemically relevant state

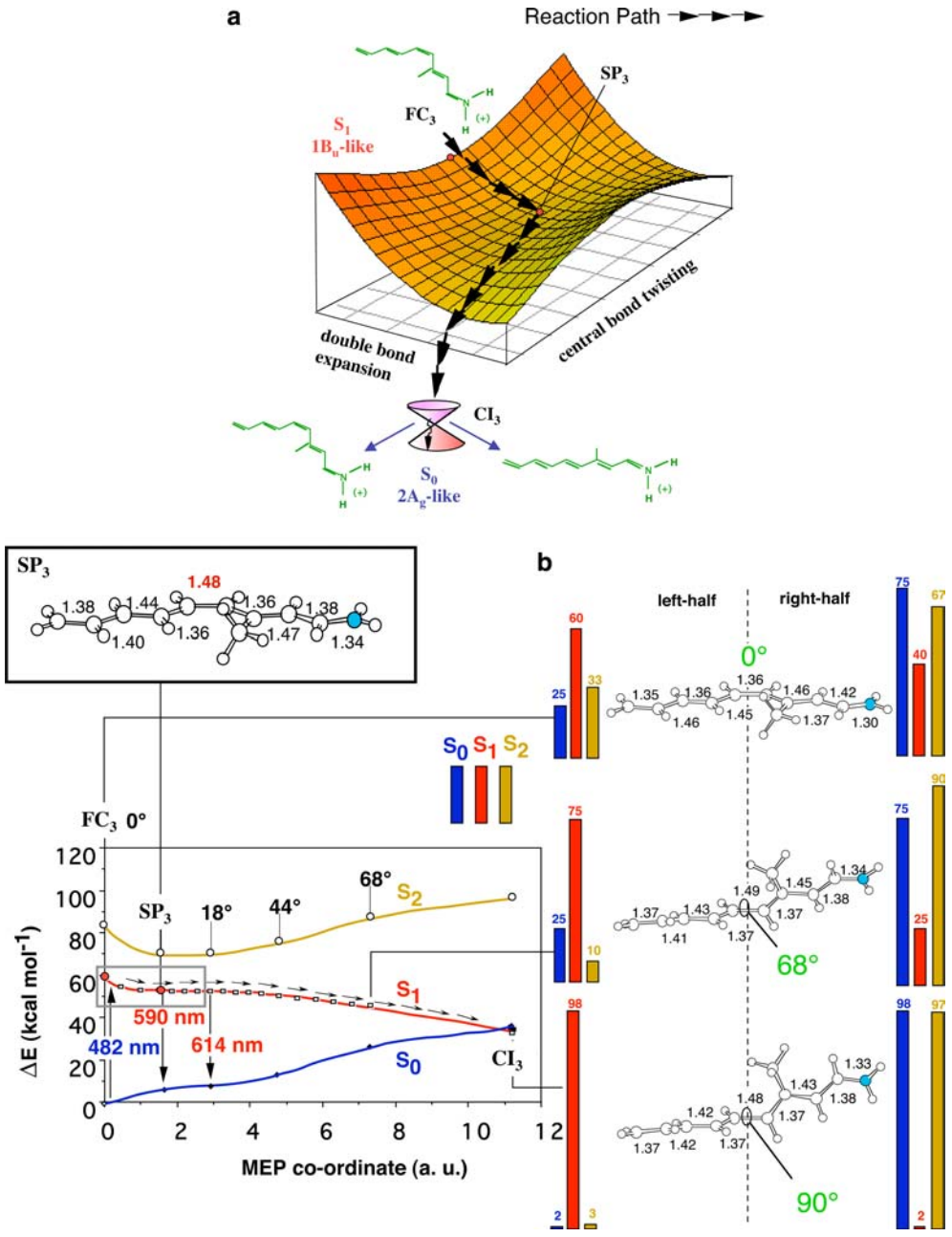

Fig. 3 **a** Schematic illustration of the two-mode structure of the S_1 ($1B_u$-like) energy surface along the excited state isomerization path for model **3**. **b** the corresponding computed MEP (scaled to match PT2 energy values), see [87]. The *grey frame* refers to the surface reported in part (**a**). The *bar diagrams* give the S_0, S_1 and S_2 (CAS-SCF 6–31G*) Mulliken charges for the $H_2C{=}CH{-}CH{=}CH{-}CH$ (*left diagrams*) and $CH{-}CH{=}CH{-}CH{=}NH_2$ (*right diagrams*) moieties. The *stream of arrows* on the S_1 surface represents the two-mode reaction co-ordinate starting at the Franck-Condon point (**FC3**). *Point* **SP3** corresponds to a flat planar stationary point on S_1 (i.e. a metastable species), where the torsional deformation leading to the degenerate $S_1 \rightarrow S_0$ decay funnel **CI3** begins. Geometrical parameters are in Å and degrees [118]

(driving the photochemistry of the system) is the spectroscopic charge-transfer state S_1 (that corresponds to the ^1B_u-like – hole-pair – spectroscopic state of polyenes). Moreover, the S_1 reaction co-ordinate along the computed barrierless photoisomerization path is curved, being sequentially dominated by two different perpendicular modes (see Fig. 3a for a schematic view of the shape of the S_1 potential energy surface of **3**). The first mode is totally symmetric (preserving the planarity of the system) and drives the initial (<50 fs) dynamics [109] out of the Franck-Condon point (FC) through a concerted double-bond expantion and single-bond compression process involving C–C bond order inversion. The second mode is asymmetric and is dominated by the *cis–trans* isomerization mode that ultimately leads to a CI featuring a 90° twisted central double bond (see Fig. 3b). The CI features a charge-transfer electronic structure corresponding to a TICT

state [85,87,90] where, substantially, a "net" electron has been transferred from the "C" to the "N" end of the skeleton and, consequently the positive charged has moved from "N" to "C". These data provide a rationale for the ultrafast radiationless decay observed in retinal chromophores.

Computed absorption and fluorescence maxima, changes in dipole moments and simulated resonance Raman spectra for model 3 [86,87,110,111] are consistent with the corresponding experimental quantities, providing a validation of the quality of the investigated models [112]: notice that the computed two-mode reaction coordinate of the S_1 relaxation path of retinal chromophores has now been validated experimentally [109,113–117] both in proteins and solvents.

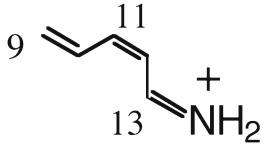

1

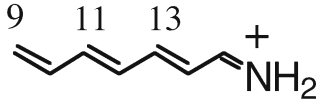

2

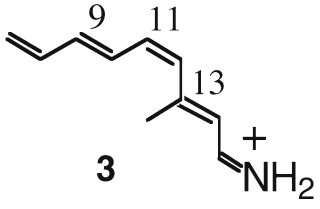

3

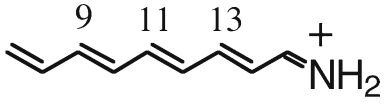

4

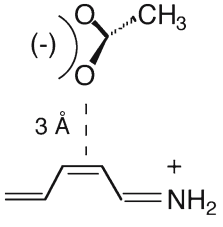

1a

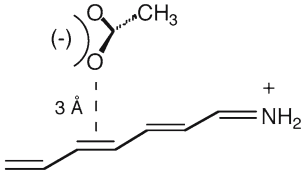

2a

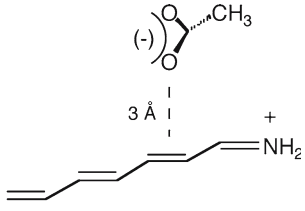

2b

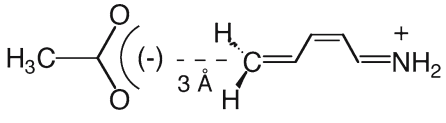

1b

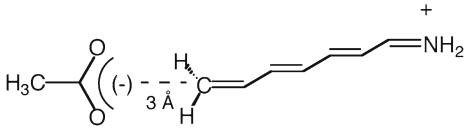

2c

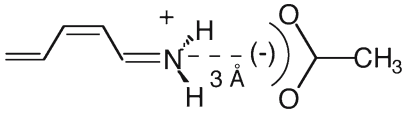

1c

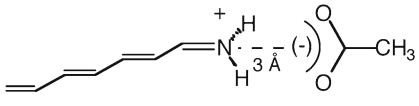

2d

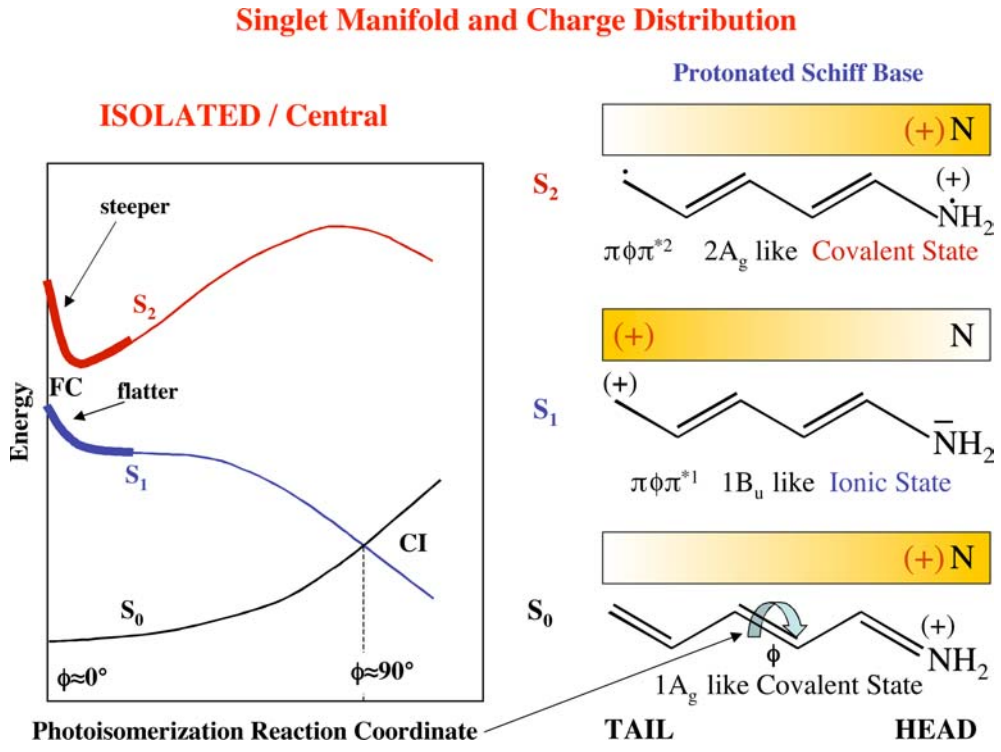

Scheme 6 Singlet manifold and charge distribution (from [118])

6.2 Counterion effects

Among others, the intermolecular interaction of the chromophore cation with its counterion (a carboxylate anion in proteins) must play a crucial role in determining the environment effects. In fact, as mentioned above, the photochemically relevant S_1 state is a "hole-pair" charge transfer state [85–87,90]. Thus its relative energy and stability with respect to the "dot–dot" S_2 and S_0 covalent states must depend on the position of the counterion relative to the chromophore backbone. Pioneering studies and first qualitative models of counterion effects on retinal PSB photochemistry are due to Weiss and Warshel [119], Sheves et al. [120,121], Nakanishi and coworkers [122–124], Honig et al. [125], Birge and Hubbard [126], Michl and Bonacic-Koutecky [55,127]. Anyway, the lack of accurate ab initio computations and systematic investigations has lead us to probe counterion effects at the CASPT2//CASSCF level for the positions/orientations defined by models **1a**, **1b**, **1c** and **2a**, **2b**, **2c**, **2d** [118]. Although the energetics delivered by these shorter retinal models may be quite different than for retinal itself, still we think we can have a qualitatively correct picture for the effects of a countercharge (an acetate placed at ca. 3 Å distance) on the photochemistry and spectral tuning of PSBs in general, as we previously showed for PSBs in vacuo. We have shown that while these results provide information on the factors responsible for (a) the relative stability of the S_0, S_1, and S_2 states; (b) the selection of the photochemically relevant excited state; (c) the excited state lifetime and reaction rate and (d) the control of the photoisomerization stereospecificity, a predictive and simple qualitative (electrostatic) model readily rationalizes the computational results providing an explanation for different aspects of the observed "environment" effect [118].

A qualitative electrostatic model. In Scheme 6 we report the structure of the singlet manifold along the computed S_1 reaction path for a PSB (here the penta-2,4-dieniminium cation has been used as a model) [85–87]. In the same scheme we also provide information on the electronic nature of the singlet (S_0, S_1, S_2) states. Accordingly, horizontal smoothed colored bars (representing the PSB skeleton) illustrate the positive charge distribution as a function of the color intensity. Note that the initial steepness of the singlet excited states is higher for the covalent state S_2 (see also Fig. 3b) [84,128].

If one places a counterion close to the chromophore, its electrostatic field will stabilize the singlet (S_0, S_1, S_2) states depending on the distance between the negative (counterion) and the positive (chromophore) charge centers. On the other hand the position of the positive charge along the PSB backbone depends on the nature of the electronic state (e.g. it is closer to the nitrogen-head (*N-head*) for covalent states and to the carbon-tail (*C-tail*) for the charge-transfer state). Thus, opposite counterion effects are expected for different states. Indeed, three different limiting cases can be envisioned:

1. The counterion is placed in a *Central* position above the chromophore backbone (1a, 2a, 2b). In this case the stabilization effect must be almost independent from the

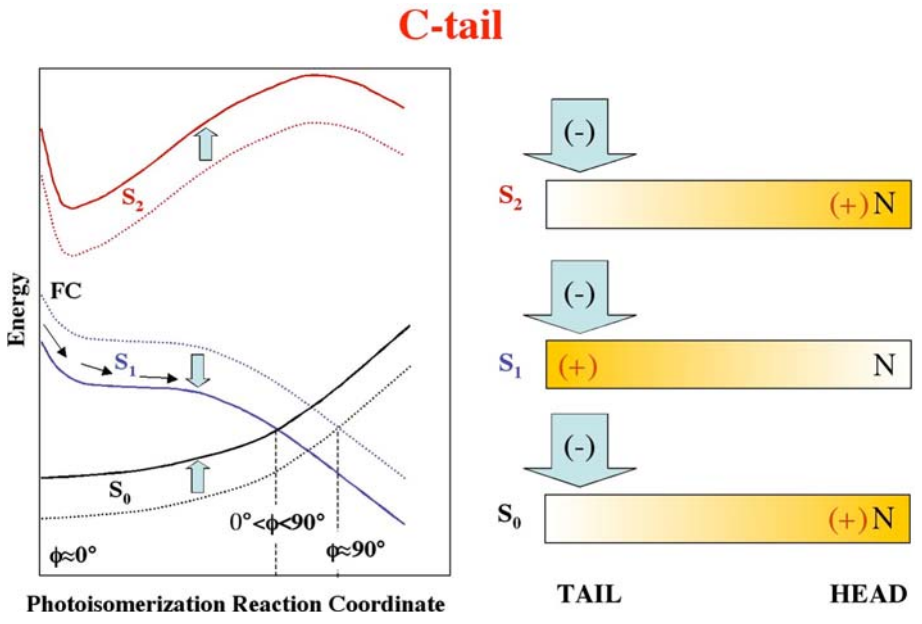

Scheme 7 (From [118])

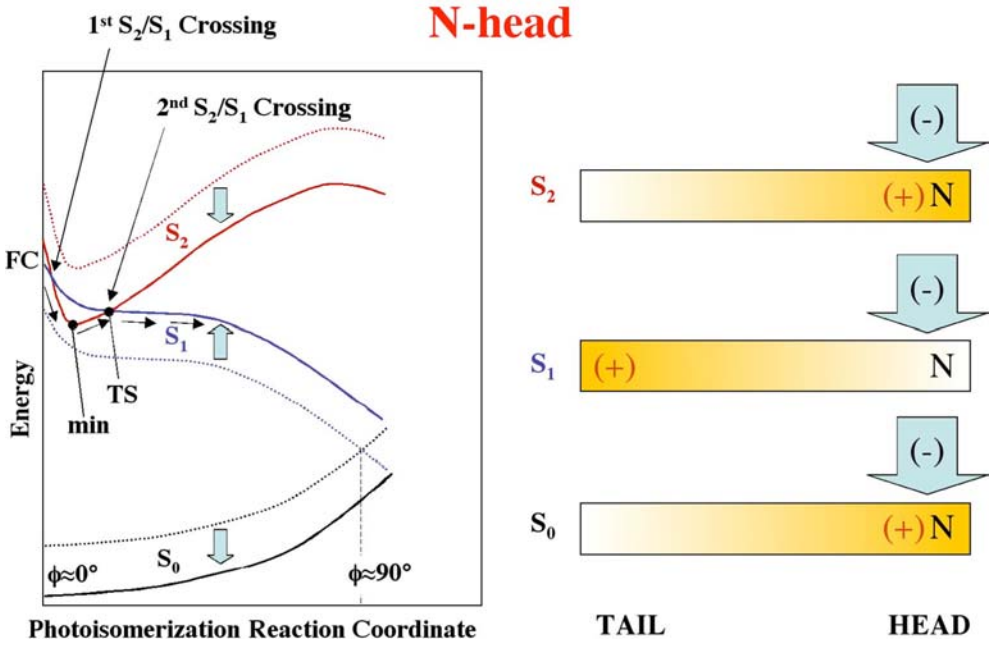

Scheme 8 (From [118])

singlet state nature (i.e. the distance between the negative and positive charges is similar for covalent and charge-transfer states). Therefore, the structure of the singlet manifold is likely to remain substantially unchanged (see Scheme 6);

2. The counterion is placed closer to the *C-tail* (**1b**, **2c**). In this position (see Scheme 7) the charge-transfer (S_1) state is stabilized (i.e. shorter couterion/positive-charge distance) with respect to the (S_0, S_2) covalent states. This leads to a change in the structure of the singlet manifold where the S_1–S_0 energy gap decreases (i.e. an absorption red shift) and the S_2–S_1 increases. Consequently (according to the intensity of this effect and the slopes of the S_1 and S_0 surfaces) the S_1/S_0 crossing should occur earlier along the S_1 isomerization path;
3. The counterion is placed closer to the *N-head* (**1c**, **2d**). In this position the covalent states (S_0, S_2) is stabilized with respect to the (S_1) charge-transfer state (see Scheme 8). This leads to a S_1–S_0 energy gap increase (i.e. absorption blue shift) and a S_2–S_1 decrease. While the S_1/S_0

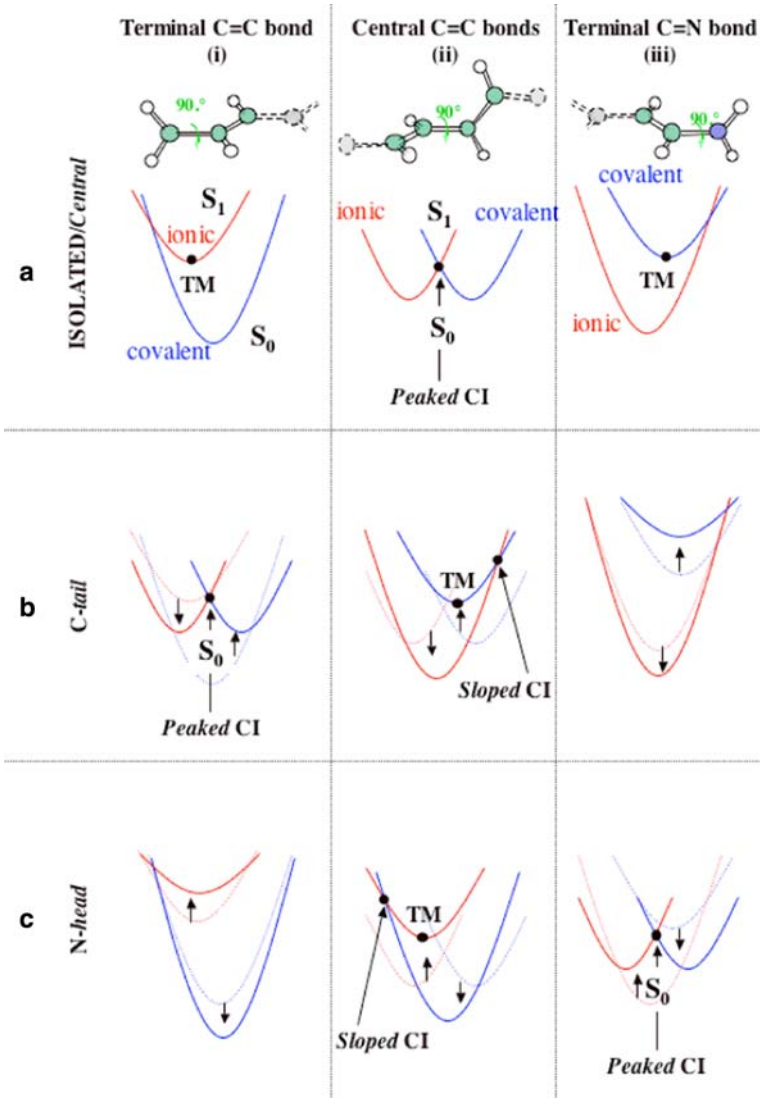

Scheme 9 (From [118])

conical intersection is expected to occur later along S_1 isomerization path, a S_2/S_1 crossing could be generated in this case as found in neutral polyenes [8,54,69,76–84] with a consequent change in the electronic structure of S_1 along the initial part of the path. Thus, while a diradical-type S_1 minimum could exist, an avoided crossing TS could emerge (due to a second S_2/S_1 crossing between the bonding covalent and antibonding ionic surfaces) along the isomerization path (see Scheme 8), which recovers the ionic (charge-transfer) nature of the S_1 state.

CASPT2//CASSCF photoisomerization path computations performed on the ion-pair model systems above, demonstrate that such behavior is indeed found, and the results are consistent with that predicted by the simple electrostatic model above.

Conical intersections versus twisted excited state intermediates. While the isomerization of the central double bonds leads to a topographically *peaked* [8,49,129] S_1/S_0 conical intersection in isolated conditions [80,85–87], the torsional deformation of the two terminal double bonds $CH_2 = CH–$ and $–CH = NH_2^+$ leads to real S_1 twisted minima (TM) [85] However, while the $CH_2 = CH–$ minima is found to correspond to a true TICT state (i.e. the electronic structure is the same seen for the conical intersection), the $–CH = NH_2^+$ minimum has a covalent electronic structure.

The effect of the position of the counterion on the S_1–S_0 energy gap at these twisted points can be easily predicted using simple potential energy curve models for the ionic charge-transfer (gray lines) and covalent (black lines) states (see Scheme 9). In Scheme 9a we report, for an isolated PSB, such model curves for the three cases (i–iii) defined above. Similarly, in Scheme 9b and 9c we report the predicted counterion effects for the *N-head* and *C-tail* positions, respectively (again, the *Central* position should leave the curves substantially unmodified, see Scheme 9a). The ionic curve

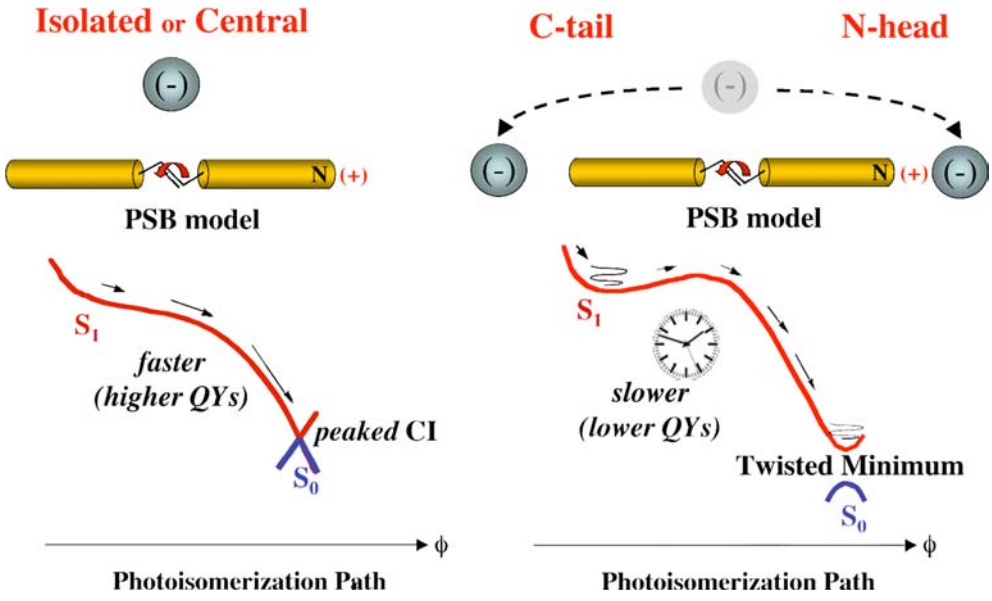

Scheme 10 (From [118])

is stabilized for the *C-tail* while destabilized for the *N-head* orientation, respectively. Accordingly, the S_1/S_0 crossing is predicted to shift to higher (or to lower) energies leading to a change in conical intersection topography from *peaked* to *sloped* [8,49,129] (or from *sloped* to *peaked*). Most importantly, such change may lead to the emergence of a twisted minimum (TM) replacing the *peaked* CI at the bottom of the S_1 energy surface. On the other hand, when the twisted double-bond gets closer to the counterion (e.g. $CH_2 = CH–$ for the *C-tail* and $–CH = NH_2^+$ for the *N-head* positions) the S_1–S_0 energy gap gets smaller and, when the magnitude of the effect is large enough, a *peaked* CI should replace the TM structure. This prediction has been validated by our computational results on the ion pairs.

7 A unified view for countercharge intermolecular effects

7.1 Reaction rate and efficiency control

All the computational results collected for the investigated ion-pairs show that the steepness along the computed photoisomerization MEP and the $S_1 - S_0$ energy gap in the twisted region can be tuned and controlled by the counterion position along the chain. Isolated systems (1 and 2) or *Central* models (1a, 2a, and 2b) display the most favored conditions for ultrafast and efficient central double bond photoisomerizations, namely: (a) steep and/or barrierless isomerization paths, and (b) TICT conical intersection points of the *peaked* type for internal C–C double-bond flip, funneling an ultrafast and efficient radiationless decay that prompts a high photoisomerization QY. In fact, no thermal equilibration is expected, nor at the initially relaxed planar point on S_1, neither at the degenerate TICT structures. On the other hand, as the countercharge is moved backward to the *C-tail* (1b, 2c) or forward to the *N-head* (1c, 2d) of the system, a slower and less efficient photoisomerization process is expected because: (a) the S_1 PES steepness along the path decreases, (b) a barrier can possibly emerge, and (c) *peaked* conical intersections for internal C–C double-bond isomerizations are replaced by twisted minima (with significant energy gap separation between S_1 and S_0) at the bottom of the computed S_1 MEP (see Schemes 6–9). Barriers and thermal equilibration at these minima would delay the process, decreasing radiationless decay rate, photoisomerization efficiency and QYs (see Scheme 10).

In conclusion, our results show that the position of the external countercharge can be used as a suitable tool to tune photoisomerization rate and efficiency: only when the countercharge is placed in a *Central* position, or its effects are quenched (i.e. isolated systems), photoisomerization efficiency is magnified and very favored ultrafast (i.e. barrierless) radiationless decay channels are opened. On the other hand, electrostatic interaction with counterions at the *N-head* or the *C-tail* would result (although for different reasons, see Sect. 4) in slower and less efficient photoisomerizations and radiationless decays.

7.2 Photoisomerization stereoselectivity control

Perhaps, one of the most remarkable computational results is that countercharge position does provide a valuable tool to select the double bond likely involved in the photoisomerization process. Moving the counterion above the molecular plane of the chromophore does effect competitive isomerizations for internal C–C double bonds (as seen in models 2a and

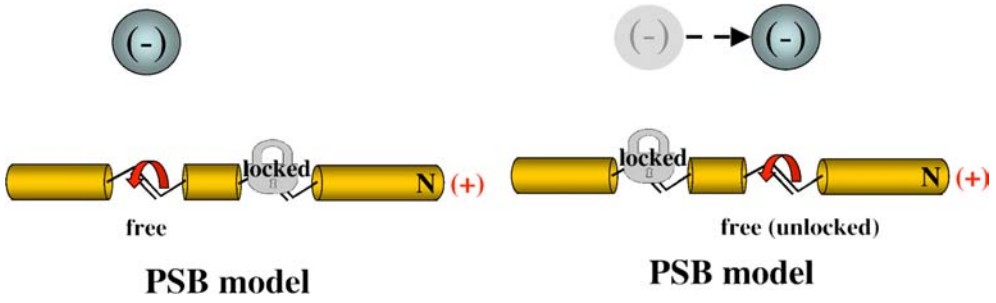

Scheme 11 (From [118])

2b), opening or locking specific isomerization paths: a barrierless (i.e. efficient) photoisomerization leading to a TICT CI point (i.e. an ultrafast radiationless decay funnel) occurs only for the double-bond being closer to the anion (i.e. the double bond right below it), while the other competitive path gets locked, or at least becomes much less favored (i.e. a barrier emerges along the path, and/or the *peaked* CI point disappears being replaced by a twisted minimum, which leads to thermal equilibrations), see Scheme 11.

An even more general result is that the *peaked* CI found in the twisted region follows the counterion along the chain of the chromophore, i.e. it involves the rotation of the double bond closer to the anion (Scheme 9 provides a qualitative explanation for that). This means that highly efficient radiationless decay channels should only exist for photoisomerizations occurring in the vicinity of the countercharge. Anyway, only for the *Central* positions (1a, 2a, and 2b) barrierless paths exist (or at least the energy barrier gets negligible), therefore opening channels for highly efficient and ultrafast photoisomerizations.

8 Rhodopsin photoreceptors at the CASPT2//CASSCF/AMBER QM/MM level

The computational results for PSB/counter ion pairs have shown (see Sect. 7) that the influence of an external charge can be quite big. Indeed, it is a well established experimental result that the environment affects different aspects of the photoisomerization process such as the rate, selectivity, efficiency, and quantum yields (QYs). For instance, in Rh (bR) the excited state PSB11 (PSBT) lifetime (following a mono-exponential decay) [130] is ca. 150 fs (200 fs) [131] and its photoisomerization takes place in 200 fs (500 fs) [132, 133] leading to the unique *all-trans* PSBT (13-*cis* PSB13) photoproduct with an high 67% (65%) QY [134]. This behavior is different from that observed for the same chromophores in solution (methanol or hexane) where, for instance, excited state lifetime follows a bi-exponential decay [130,135] with a dominant (almost 20 fold longer) 3 ps shorter component [136] and there is a lack of stereospecificity and a decrease in the photoisomerization efficiency (to a low 25% QY) [137, 138]. It is thus apparent that the protein is able to "catalyze" (i.e. speed up and select) the photoisomerization with respect to the solution environment.

To allow this investigation to be achieved, we have developed (see Sect. 3 and [75] for the details) and employed a CASSCF/AMBER QM/MM force filed. This method, when complemented with multi-reference CASPT2 computations to account for correlation energy, allows sizable systems of biological relevance (such as rhodopsin photoreceptors) to be investigated at an unprecedented level of accuracy.

The results of the computational QM/MM investigation of photoinduced isomerizations in Rh and bR have been published very recently. The S_1/S_0 intersection space (IS) inside the protein has been mapped for both photoreceptors, and an extended IS segment has been located right at the bottom of the S_1 surface spanning structures for the chromophore not observed in vacuo. In particular, the analysis of these results indicates that photochemical funnels mediating competing Z/E photoisomerizations of the retinal chromophore, reside in the same IS. While this question may appear to be of purely theoretical interest, it is in fact not so since IS segments connecting low-lying chemically distinct CI may play a role in the environmental or substituent control of the reaction selectivity. The fact that there are low-lying IS segments featuring regions controlling distinct chemical reactions, suggests that the knowledge of the detailed topology and topography of the $n-2$ dimensional IS is of importance for the comprehension of substituent or catalytic effects or, more generally, of the fine tuning of the photochemical reactivity. This knowledge becomes crucial when we wants to control the photochemical properties of the chromophore through a proper design of the chromophore itself as well as of the chemical environment surrounding it, as it occurs in supramolecular chemistry.

All the key structures involved in the primary event of the ultrafast photoinduced isomerization of the retinal chromophore in Rh (i.e. the FC point, the fluorescent structure on the excited state S_1, the twisted C=C central double bond S_1/S_0 decay funnel, the primary photoproduct) and their spectroscopic features have also been simulated via this QM/MM approach, and compared to the QM/MM computational results for the same process in solvent [139]. Very remarkably, the results nicely agree with the available experimental data in the two environments, allowing this biologically relevant process to be characterized at such an accurate and reliable level for the first time.

9 Conclusions and perspectives

Above we have shown how the computational description of a photochemical organic reaction co-ordinate, *from energy absorption to photoproduct formation*, has become technically feasible nowadays: Tools have been developed and a protocol has been implemented, which allows a systematic computational analysis of a photochemical process to be achieved with an unprecedentedly detailed view. The conceptual problems that need to be solved in order to apply quantum chemistry to photochemical problems relate mainly to the computation of the MEP and the characterization of the CI funnels. As clearly shown in our works and pointed out in recent reviews [7,8,37,49,56], CIs are far from being an abstract feature of quantum chemistry, since they represent ubiquitous key mechanistic elements in photochemical reactions. For example, it has been shown that the photoisomerization of retinal PSB involves a conical intersection. This is intimately connected to the process of vision and, therefore, to an everyday life photobiological event. We have pointed out their experimental implications: the branching of the reaction path occurring at such crossing points, as well as the stereochemistry following from their structures (photochemical reaction pathways getting through conical intersections have a stereochemistry which is driven by their electronic and structural properties).

The electronic factors playing a role in the stability and selection of the low-energy conical intersections which drive the photochemistry of nonpolar and highly polar (i.e. PSB) conjugated hydrocarbons in isolated conditions (i.e. in vacuo) have been analyzed and a unified and unambiguous view has been provided of their *intrinsic* photochemical reactivity. The effects of external charges have also been investigated in order to have a first insight into environmental effects. Both stereoselective and rate/efficiency effects on the photoinduced processes have been detected and a rationale has been presented in terms of simple electronic/electrostatic-based models.

One of the tasks of such a detailed investigation is to provide chemists with a systematic bunch of information that might be relevant in molecular technology giving a valuable guideline for the control of photoinduced processes and for the design of artificial photo-switchable devices. In fact, both the environment and the chromophore structure may be exploited to tune the photochemical reactivity and efficiency. For example, it has been shown how the position and the distance of the countercharge in a PSB/counter ion pair seem to be a valuable tool for tuning photoisomerization rate, efficiency and stereoselectivity.

A major step towards reality has been very recently achieved through the development and the use of a new hybrid QM/MM CASPT2//CASSCF/AMBER force field: this allows organic chromophores in realistic conditions (e.g. solvent, protein, etc.) to be investigated at an unprecedented level of accuracy. We are just at the beginning of this fascinating field of research. Expectations are very much intriguing indeed, dealing for the first time with the promise of a very accurate description of the photochemical reactivity involving a complex organic system in *realistic conditions*, such as chromophores embedded in modified protein cavities, or artificial functionalized bio-mimetic environments, or solvents or, finally, supramolecular structures. Still, more efficient optimization strategies and mapping procedures have to be foreseen and implemented for sizable systems, but we expect big improvements and outstanding results in the near future, concurrently with the development of these new tools and new atom-link approaches allowing a more accurate simulation of the QM–MM frontier, thus leading to more reliable QM/MM methods. We have also seen how different low-lying conical intersections featuring regions controlling distinct chemical reactions exist for the same organic chromophore. This suggests that the knowledge of the detailed topology of the intersection space is of importance for the comprehension of the photochemical reactivity in general, including dynamics effects, and its environmental dependent tuning. This strongly calls for efficient and rigorous tools to explore systematically the intersection space (e.g. for the optimization of transition structures and saddle points, besides the simple optimization of minima, and for the computation of MEP inside this region). Regrettably, these methods are not yet available, and we think that the formulation and implementation of such tools will constitute a significant step forward in the field of computational photochemistry.

In conclusion, we believe that all the aforementioned embodies a prominent achievement towards a comprehensive understanding of photochemical processes in organic systems, furthermore providing a valuable instrument for the prediction of photo-induced reactions and the design of photo-driven molecular devices that is the final goal of every photochemist. Furthermore, new areas of promising research have been identified, which should be pursued and developed. This will allow a deeper insight into photoinduced events for sizable systems of biological/technological relevance to be achieved to unprecedented accuracy and detail.

References

1. Drexler KE (1986) Engines of creation: the coming era of nanotechnology. Anchor, New York, USA
2. Dugave C, Demange L (2003) Chem Rev 103:2475
3. Tamai N, Miyasaka H (2000) Chem Rev 100:1875–1890
4. Yokoyama Y (2000) Chem Rev 1000:1717–1739
5. Irie M (2000) Chem Rev 100:1685–1716
6. Truhlar DG, Gordon MS (1990) Science 249:491
7. Fuss W, Lochbrunner S, Muller AM, Schikarski T, Schmid WE, Trushin SA (1998) Chem Phys 232:161–174
8. Robb MA, Garavelli M, Olivucci M, Bernardi F (2000) Rev Comput Chem 15:87–146
9. Punwong C, Owens J, Martinez TJ (2005) Biophys J 88:530A-A
10. Balzer B, Stock G (2005) Chem Phys 310:33–41
11. Jasper AW, Truhlar DG (2005) J Chem Phys 122:044101
12. Roman E, Martens CC (2004) J Chem Phys 121:11572–11580
13. Toniolo A, Thompson AL, Martinez TJ (2004) Chem Phys 304:133–145
14. Jasper AW, Zhu CY, Nangia S, Truhlar DG (2004) Faraday Discuss 127:1–22

15. Toniolo A, Olsen S, Manohar L, Martinez TJ (2004) Faraday Discuss 127:149–163
16. Worth GA, Robb MA, Burghardt I (2004) Faraday Discuss 127:307–323
17. Worth GA, Cederbaum LS (2004) Ann Rev Phys Chem 55:127–158
18. Ko C, Levine B, Toniolo A, Manohar L, Olsen S, et al (2003) J Am Chem Soc 125:12710–12711
19. Balzer B, Hahn S, Stock G (2003) Chem Phys Lett 379:351–358
20. Balzer B, Dilthey S, Hahn S, Thoss M, Stock G (2003) J Chem Phys 119:4204–4215
21. Schultz T, Quenneville J, Levine B, Toniolo A, Martinez TJ, et al (2003) J Am Chem Soc 125:8098–8099
22. Baeck KK, Martinez TJ (2003) Bull Korean Chem Soc 24:712–716
23. Ben-Nun M, Martinez TJ (2002) In: Advances in chemical physics, vol 121. pp 439–512
24. Hack MD, Wensmann AM, Truhlar DG, Ben-Nun M, Martinez TJ (2001) J Chem Phys 115:1172–1186
25. Ben-Nun M, Martinez TJ (2000) Chem Phys 259:237–248
26. Ben-Nun M, Quenneville J, Martinez TJ (2000) J Phys Chem A 104:5161–5175
27. Ben-Nun M, Martinez TJ (2000) J Am Chem Soc 122:6299–6300
28. Ben-Nun M, Martinez TJ (2000) J Chem Phys 112:6113–6121
29. Ben-Nun M, Martinez TJ (1999) J Phys Chem A 103:10517–10527
30. Nakamura H, Truhlar DG (2002) J Chem Phys 117:5576–5593
31. Nakamura H, Truhlar DG (2001) J Chem Phys 115:10353–10372
32. Atchity GJ, Ruedenberg K (1999) J Chem Phys 111:2910–2920
33. Atchity GJ, Ruedenberg K (1999) J Chem Phys 110:4208–4212
34. Atchity GJ, Ruedenberg K (1997) Theor Chem Acc 97:47–58
35. Ruedenberg K, Atchity GJ (1993) J Chem Phys 99:3799–3803
36. Atchity GJ, Xantheas SS, Ruedenberg K (1991) J Chem Phys 95:1862–1876
37. Fuss W, Kompa KL, Lochbrunner S, Muller AM (1997) Chem Phys Phys Chem 101:500–509
38. Lawley KP (ed) (1987) Ab initio methods in quantum chemistry - I, vols 67. Wiley, Chichester, England
39. Lawley KP (ed) (1987) Ab initio methods in quantum chemistry - II, vols 69. Wiley, Chichester, England
40. Roos BO (1987) In: Lawley KP (ed) ab initio methods in quantum chemistry - II. Wiley, New York, pp 399–446
41. Roos BO (1980) Int J Quantum Chem 14:175
42. Siegbahn PEM, Almlof J, Heiberg A, Roos BO (1981) J Chem Phys 74:2384
43. Frisch MJ, Trucks GW, Schlegel HB, Scuseria GE, Robb MA, et al (1998) Gaussian 98. Gaussian Inc, Pittsburgh
44. Andersson K, Blomberg MRA, Fülscher MP, Karlström G, Lindh R, et al (1999) MOLCAS. Lund University, Lund
45. Andersson K, Malmqvist P-Å, Roos BO (1992) J Chem Phys 96:1218
46. McDouall JJW, Peasley K, Robb MA (1988) Chem Phys Lett 148:183–189
47. Finley J, Malmqvist PA, Roos BO, Serrano-Andrés L (1998) Chem Phys Lett 288:299–306
48. Nakano H, Uchiyama R, Hirao K (2002) J Comput Chem 23:1166–1175
49. Bernardi F, Olivucci M, Robb MA (1996) Chem Soc Rev 25:321
50. Yarkony DR (1996) J Phys Chem 100:18612
51. Yarkony DR (1998) Acc Chem Res 31:511
52. Desouter-Lecomte M, Lorquet JC (1979) J Chem Phys 71:4391
53. Gilbert A, Baggott J (1991) Essentials of Molecular Photochemistry. Blackwell, Oxford
54. Klessinger M, Michl J (1994) Excited states and photochemistry of organic molecules. VCH Publishers, New York
55. Michl J, Bonacic-Koutecky V (1990) Electronic aspects of organic photochemistry. Wiley, New York
56. Bernardi F, Olivucci M, Michl J, Robb MA (1997) The Spectrum 9:1
57. Natansohn A, Rochon P (2002) Chem Rev 102:4139
58. Hampp N (2000) Chem Rev 100:1755
59. Van der Lugt WTAM, Oosterhoff LJ (1969) J Am Chem Soc 91:6042
60. Zimmerman HE (1966) J Am Chem Soc 88:1566
61. Teller E (1969) Israelian J Chem 7:227
62. Michl J (1972) Mol Photochem 4:243
63. Garavelli M, Bernardi F, Robb MA, Olivucci M (2002) Int J Photoenergy 4:57–68
64. Truhlar DG, Mead CA (2003) Phys Rev A 68:32501
65. Bearpark MJ, Robb MA, Schlegel HB (1994) Chem Phys Lett 223:269–274
66. Gonzalez C, Schlegel HB (1990) J Phys Chem 94:5523
67. Foresman JB, Aeleen F (1996) Exploring chemistry with electronic structure methods. Gaussian Inc, Pittsburgh
68. Schlegel HB (1987) In: Lawley KP (ed) Ab initio methods in quantum chemistry. Wiley, New York, pp 249–286
69. Garavelli M, Celani P, Fato M, Bearpark MJ, Smith BR, et al (1997) J Phys Chem A 101:2023–2032
70. Celani P, Robb MA, Garavelli M, Bernardi F, Olivucci M (1995) Chem Phys Lett 243:1–8
71. Pu JZ, Gao JL, Truhlar DG (2004) J Phys Chem A 108:632–650
72. Gao JL, Truhlar DG (2002) Ann Rev Phys Chem 53:467–505
73. Mo YR, Alhambra G, Gao JL (2000) Acta Chimica Sinica 58:1504–1510
74. Bayly CI, Cieplak P, Cornell WD, Kollman PA (1993) J Phys Chem 97:10269
75. Ferré N, Cembran A, Garavelli M, Olivucci M (2004) Theor Chem Acc (in press)
76. Hudson BS, Kohler BE, Schulten K (1982) In: excited states. Academic Press, New York, pp 1–99
77. Celani P, Garavelli M, Ottani S, Bernardi F, Robb MA, Olivucci M (1995) J Am Chem Soc 117:11584–11585
78. Garavelli M, Smith BR, Bearpark MJ, Bernardi F, Olivucci M, Robb MA (2000) J Am Chem Soc 122:5568–5581
79. Garavelli M, Celani P, Bernardi F, Robb MA, Olivucci M (1997) J Am Chem Soc 119:11487–11494
80. Garavelli M, Bernardi F, Olivucci M, Vreven T, Klein S, et al (1998) Faraday Discuss 110:51–70
81. Garavelli M, Frabboni B, Fato M, Celani P, Bernardi F, et al (1999) J Am Chem Soc 121:1537–1545
82. Garavelli M, Page CS, Celani P, Olivucci M, Schmid WE, et al (2001) J Phys Chem A 105:4458–4469
83. Garavelli M, Bernardi F, Olivucci M, Bearpark MJ, Klein S, Robb MA (2001) J Phys Chem A 105:11496–11504
84. Fuss W, Haas Y, Zilberg S (2000) Chem Phys 259:273–295
85. Garavelli M, Celani P, Bernardi F, Robb MA, Olivucci M (1997) J Am Chem Soc 119:6891–6901
86. Garavelli M, Vreven T, Celani P, Bernardi F, Robb MA, Olivucci M (1998) J Am Chem Soc 120:1285–1288
87. Gonzalez-Luque R, Garavelli M, Bernardi F, Merchan M, Robb MA, Olivucci M (2000) Proc Natl Acad Sci USA 97:9379–9384
88. Ruiz DS, Cembran A, Garavelli M, Olivucci M, Fuss W. (2002) Photochem Photobiol 76:622–633
89. Garavelli M, Celani P, Yamamoto N, Bernardi F, Robb MA, Olivucci M (1996) J Am Chem Soc 118:11656–11657
90. Garavelli M, Bernardi F, Celani P, Robb MA, Olivucci M (1998) J Photochem Photobiol A-Chem 114:109–116
91. Gerhartz W, Poshusta RD, Michl J (1977) J Am Chem Soc 99:4263–4271
92. Garavelli M, Bernardi F, Moliner V, Olivucci M (2001) Angewandte Chemie-International Edition 40:1466–1468
93. Garavelli M, Bernardi F, Cembran A, Castano O, Frutos LM, et al (2002) J Am Chem Soc 124:13770–13789
94. Palmer IJ, Ragazos IN, Bernardi F, Olivucci M, Robb MA (1993) J Am Chem Soc 115:673–682
95. Gilbert A (1995) In: Horspool WM, Song P-S (eds) CRC handbook of organic photochemistry and photobiology. CRC Press, Boca Raton, pp 229–236
96. Hopf H, Lipka H, Traetteberg M (1994) Angewandte Chemie-International Edition in English 33:204–205
97. Maier G (1988) Angewandte Chemie-International Edition 27: 309–335

98. Bryce-Smith D, Gilbert A (1976) Tetrahedron 32:1309
99. Zimmermann HE, Grunewald GL (1966) J Am Chem Soc 88:183–186
100. Zimmermann HE, Iwamura H (1970) J Am Chem Soc 92:2015–2022
101. Turro NJ, Liu J-M, Zimmerman HE, Factor RE (1980) J Org Chem 45:3511–3513
102. Kandori H, Shichida Y, Yoshizawa T (2001) Biochem-Moscow 66:1197–1209
103. Needleman R (1995) In: Horspool WM, Song P-S (eds) CRC handbook of organic photochemistry and photobiology. CRC Press, Boca Raton, pp 1508–1515
104. Ottolenghi M, Sheves M (1995) Israel J Chem 35:U3-U
105. Wald G (1968) Science 162:230–239
106. Mathies R, Lugtenburg J (2000) In: Stavenga DG, DeGrip WJ, Pugh ENJ (eds) Molecular mechanism of vision. Elsevier, New York, pp 55–90
107. Yoshizawa T, Kuwata O (1995) In: Horspool WM, Song P-S (eds) CRC handbook of organic photochemistry and photobiology. CRC Press, Boca Raton, pp 1493–1499
108. De Vico L, Page CS, Garavelli M, Bernardi F, Basosi R, Olivucci M (2002) J Am Chem Soc 124:4124–4134
109. Ruhman S, Hou BX, Friedman N, Ottolenghi M, Sheves M (2002) J Am Chem Soc 124:8854–8858
110. Garavelli M, Negri F, Olivucci M (1999) J Am Chem Soc 121:1023–1029
111. Cembran A, Bernardi F, Olivucci M, Garavelli M (2003) J Am Chem Soc 125:12509–12519
112. One possible reason for the success of model 3 is that retinal PSB11 has a highly twisted (ca. 60°) β-ionone ring both in solution (see Albeck A, Livnah N, Gottlieb H, Sheves M (1992) J Am Chem Soc 114:2400) and in Rh (see Teller DC, Okada T, Behnke CA, Palczewski K, Stenkamp RE (2001) Biochemistry 40:7761–7772) This prevents efficient conjugation of the β-ionone double bond with the rest of the conjugated chain, making 3 a realistic model for retinal PSBs
113. Kobayashi T, Saito T, Ohtani H (2001) Nature 414:531–534
114. Hou B, Friedman N, Ruhman S, Sheves M, Ottolenghi M (2001) J Phys Chem B 105:7042–7048
115. Haran G, Morlino EA, Matthes J, Callender RH, Hochstrasser RM (1999) J Phys Chem A 103:2202–2207
116. Logunov SL, Volkov VV, Braun M, El-Sayed MA (2001) Proc Natl Acad Sci USA 98:8475–8479
117. Kandori H, Furutani Y, Nishimura S, Shichida Y, Chosrowjan H, et al (2001) Chem Phys Lett 334:271–276
118. Cembran A, Bernardi F, Olivucci M, Garavelli M (2004) J Am Chem Soc 126:16018–16037
119. Weiss RM, Warshel A (1979) J Am Chem Soc 101:6131–6133
120. Sheves M, Kohne B, Mazur J (1983) J Chem Soc, Chemical Commun:1232–1234
121. Sheves M, Nakanishi K, Honig B (1979) J Am Chem Soc 101:7086–7088
122. Nakanishi K, Balogh-Nair V, Arnaboldi M, Tsujimoto K, Honig B (1980) J Am Chem Soc 102:7945–7947
123. Motto MG, Sheves M, Tsujimoto K, Balogh-Nair V, Nakanishi K (1980) J Am Chem Soc 102:7947–7949
124. Honig B, Dinur U, Nakanishi K, Balogh-Nair V, Gawinowicz MA, et al (1979) J Am Chem Soc 101:7084–7086
125. Honig B, Greenberg AD, Dinur U, Ebrey TG (1976) Biochemistry 15(21):4593
126. Birge RR, Hubbard LM (1980) J Am Chem Soc 102:2195–2205
127. Bonacic-Koutecky V, Koutecky J, Michl J (1987) Angewandte Chemie-International Edition 26:170–189
128. There is general agreement of all multi reference methods that the covalent state energy is reduced much faster during geometrical relaxation: (a) Strodel P, Tavan P (2002) J Chem Phys 117:4677. (b) Nakayama K, Nakano H, Hirao K (1998) Int J Quantum Chem 66:157
129. Atchity GJ, Xantheas SS, Ruedenberg K (1991) J Chem Phys 95:1862
130. Hamm P, Zurek M, Roschinger T, Patzelt H, Oesterhelt D, Zinth W (1996) Chem Phys Lett 263:613–621
131. Kandori H, Sasabe H, Nakanishi K, Yoshizawa T, Mizukami T, Shichida Y (1996) J Am Chem Soc 118:1002–1005
132. Schoenlein RW, Peteanu LA, Mathies RA, Shank CV (1991) Science 254:412–415
133. Mathies RA, Cruz CHB, Pollard WT, Shank CV (1988) Science 240:777–779
134. Dartnall HJA (1967) Vis Res 8:339–358
135. Logunov SL, Song L, ElSayed MA (1996) J Phys Chem 100:18586–18591
136. Kandori H, Katsuta Y, Ito M, Sasabe H (1995) J Am Chem Soc 117:2669–2670
137. Becker RS, Freedman KA (1985) J Am Chem Soc 107:1477–1485
138. Koyama Y, Kubo K, Komori M, Yasuda H, Mukai Y (1991) Photochem Photobiol 54:433–443
139. Andruniow T, Ferré N, Olivucci M (2004) Proc Natl Acad Sci USA 101:17908–17913